https://doi.org/10.48048/tis.2022.6173

Optical and Photovoltaic Properties of New Synthesized Quinoxaline-2,3 Dione Derivatives for Efficient Dye Sensitized Solar Cell Application

Abdeslam El Assyry[1,*], Issam Rafiq[1], Mohamed Rbaa[2], Abdelali Derouiche[1] and Brahim Lakhrissi[2]

[1]Laboratory of Polymer Physics, Mechanical Sciences and Materials, Department of Physics, Faculty of Science Ben M'Sik, Hassan II University, Casablanca, Morocco
[2]Laboratory of Organic Chemistry, Catalysis and Environment, Department of Chemistry, Faculty of Science, Ibn Tofail University, Kenitra, Morocco

([*]Corresponding author's e-mail: abdeslam_elassyry@yahoo.fr)

Received: 7 May 2021, Revised: 6 August 2021, Accepted: 17 August 2021

Abstract

In this study, the synthesis of 4 new heterocyclic compounds derived from quinoxalinedione were presented, which have been characterized by ^{1}H and ^{13}C NMR spectroscopy. The solar cells' photovoltaic properties based on these novels organic compounds donor-π-acceptor dyes were studied. Density functional theory DFT method is realized to optimize electronic parameters, optical and photovoltaic properties for some new 8-hydroxyquinoline derivatives based on quinoxaline-2,3-dione. The results have shown that time-dependent DFT (TDDFT) investigations with polarizable continuum model PCM were significantly able to foretell the excitation energy and the spectroscopy of the molecule. The highest occupied molecular orbital HOMO and the lowest unoccupied molecular orbital LUMO energy levels of these molecules can ensure a positive impact on the dye regeneration and electron injection process. Injection driving force ΔG^{inject}, light-harvesting efficiency LHE, reorganization energy λ_{total} and open-circuit photovoltage V_{oc} provide qualitative predictions on these dyes' reactivity. Among these 4 molecules, the compounds which can be used as organic solar cells have determined.

Keywords: Optical, Photovoltaic, Quinoxalinedione, PCM, TD-DFT

Introduction

The quinoxalinedione derivatives have attracted attention in several molecular applications [1-4]. Synthesis, energetic and structural properties of some quinoxalinedione derivatives were made by our group [5-10]. Spectroscopic data are in agreement with literature [5,8,10]. Organic photovoltaic solar cells (OPVSC) pose an important potential for progress in the work for electricity production from low-cost compounds. In the last years, we have noticed a significant growth in the (OPVSC) conversion efficiency [11,12]. Some technical aspects were presented whose objective is to minimize the costs of photovoltaic compounds, thus extending a technology based on environmentally friendly materials. This objective is becoming achievable continuously in the high-performance organic screen evolution in the electronics industry [13-15].

Some Quinoxaline-based polymers have received an attention lot for their flexibility, processing ease, weak weight and their production weak cost [16-18]. Relatively, their large band gaps limited the short-circuit current density (J_{sc}), reducing the power conversion efficiencies (PCE); this last one is based on the open-circuit photovoltage (V_{oc}), the J_{sc}, and the fill factor (*FF*) systems. Low band-gap conjugated polymers (CP) have been developed to best match the solar spectrum and so produce a higher J_{sc} [19]. Now, the organic solar cell photoelectric conversion efficiency is well over 7 % [20,21]. Thus, the new improvement of the (PCE) requires the development of new (CP) with greater absorption and adequate energy levels along the solar spectrum. Therefore, the heavy load carrier mobility of semiconductor polymers must be tokening into account [22,23]. The photo-excitation process in conjugated systems cannot generate free charge carriers but neutral, bound electron-hole pairs so that charge transfer might facilitate the formation of free charge carriers [23]. Intermolecular charge transfer has been known to be short distance process in

the organic conjugated materials. The method used only gives the HOMO to LUMO charge transfer so that usually it is only applicable to the lowest excited state and other charge transfer contributions are neglected.

The experimental results reached for organic molecules without minerals remain limited to date. As some of the studies works only searched the optoelectronic and photophysical properties for dye sensitizers [24,25], also intra molecule e^--dynamic process between compounds and TiO_2 [26,27]. The central quinoxalinedione has been paired to (CH_3, Cl, NO_2 and hydroxiquinolinyl), and bonded to the substituent as an Acceptor/anchor group forming D-π-A designing. The optical absorption and e^--structural properties were calculated of 4 dye sensitizers D_i(I = 1 - 4) **Figure 1**. As well, the various electron-donor (e^--D) group role has been analyzed in the structures setting. In this work, we searched to see the sensitizer donor impacts on the open-circuit photovoltage (V_{oc}) and the short-circuit current density (J_{sc}) of the cell through discussing the key factors affecting V_{oc} and J_{sc} with the goal of finding potential sensitizers for use in dye-sensitized solar cell (DSSC).

D1: 1,4-Bis((8-hydroxyquinolin-5-yl)methyl)quinoxaline-2,3(1H,4H)-dione.
D2: 1,4-Bis((8-hydroxyquinolin-5-yl)methyl)-6-methylquinoxaline-2,3(1H,4H)-dione.
D3: 6-Chloro-1,4-bis((8-hydroxyquinolin-5-yl)methyl)quinoxaline-2,3(1H,4H)-dione.
D4: 1,4-Bis((8-hydroxyquinolin-5-yl)methyl)-6-nitroquinoxaline-2,3(1H,4H)-dione.

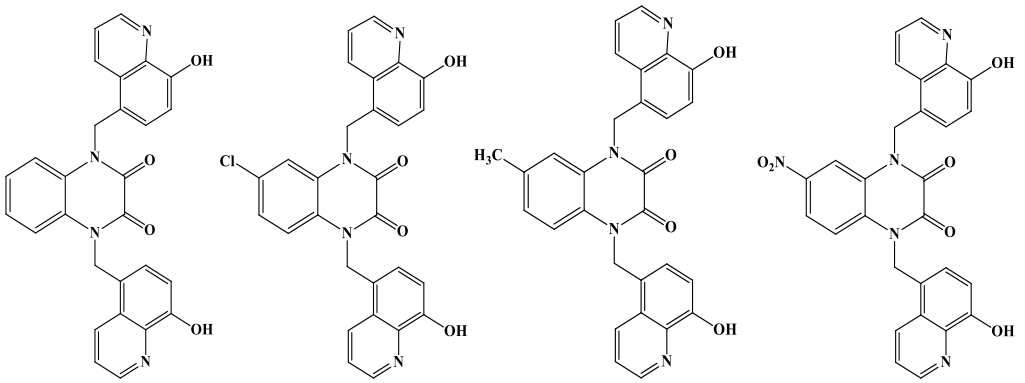

D1 ($C_{28}H_{20}N_4O_4$) **D2** ($C_{29}H_{22}N_4O_4$) **D3** ($C_{28}H_{19}N_4O_4Cl$) **D4** ($C_{28}H_{19}N_5O_6$)

Figure 1 Optimized geometries of all the compounds used.

Theoretical

Theoretical background

The cell current-voltage characteristics design in the dark and under lighting, allows evaluating more of its electrical behavior and its PV performances [28,29]. Fill factor *FF*, Incident photon to current efficiency *IPCE* and External photovoltaic yield η are determining by:

$$FF = \frac{P_{\max}}{V_{oc} \times I_{sc}} = \frac{V_{\max} \times I_{\max}}{V_{oc} \times I_{sc}} \quad (1)$$

$$IPCE = \frac{J_{sc}}{G \times \lambda} \times \frac{hc}{e} \quad (2)$$

$$\eta = \frac{P_{\max}}{S \times G} = FF.\frac{I_{sc}.V_{co}}{P_{inc}} \quad (3)$$

in which; $P_{\max}$ the maximum power issued by the photovoltaic cell (PVC); G the illumination; S the surface and P_{inc} is the incident solar power on the cell.

For cell productivity, the conversion yield is very important [30]; an ideal cell can be subject to the following thermionic injection model [31]:

$$I = I_s\left(\exp\left(\frac{eV}{kT}-1\right)\right) \quad (4)$$

and

$$J_{sc} = \int_{\lambda} LHE(\lambda)\Phi_{inject}\eta_{collect}d\lambda \quad (5)$$

or I_s : Saturation current in inverse polarization, Φ_{inject} : Electron injection efficiency, $\eta_{collect}$: Charge collection efficiency and $\eta_{collect}$ = Constant.

For high J_{sc}, the efficient sensitizers used in DSSC must have to high light-harvesting efficiency (*LHE*). As we calculated the *LHE*, Φ_{inject} and λ_{total} to make light on the link enter J_{sc} and η.

The *LHE*, ΔG^{inject} and E^{dye*} are determined by [32]:

$$LHE = 1 - 10^{-f} \quad (6)$$

$$\Delta G^{inject} = E^{dye*} + E_{CB} \quad (7)$$

$$E^{dye*} = E^{dye} - E_{00} \quad (8)$$

where E^{dye} and E^{dye*} are the compound oxidation potential energy in the ground and excited state, E_{CB} is the reduction potential of the TiO_2 conduction band, E_{00} is an electronic vertical transition energy associate to λ_{max} and f is the oscillator force corresponding to λ_{max}. We establish that the larger f would have the greater light-harvesting efficiency. So, in a few works the value E_{CB} = –4.0 eV for TiO_2 is broadly used [33-36], E^{dye*} can be determined [35-37].

The precedents papers signed that the investigation with an unrelaxing path is efficient [28,32]. So, the e^- injection from the compound excited state to the TiO_2 conduction band is given by an unrelaxing path in our calculation. Thus, the small λ_{total} which contains the hole reorganization energy λ_h and the electron reorganization energy λ_e could improve the J_{sc}, λ_h and λ_e are determined by [38]:

$$\lambda_i = \left(E_0^{\pm} - E_{\pm}^{\pm}\right) + \left(E_{\pm}^{0} - E_0\right) \quad (9)$$

where $E_0^{\pm}$, $E_{\pm}^{\pm}$, $E_{\pm}^{0}$ and E_0 are well known and determined energy recently [39].

Figure 2 present the idealized equivalent circuit, which is an absolute current generator. In which, R_s and R_{sh} are the series and shunt resistances, R_L is the external circuit charge resistance and I_L is a current source.

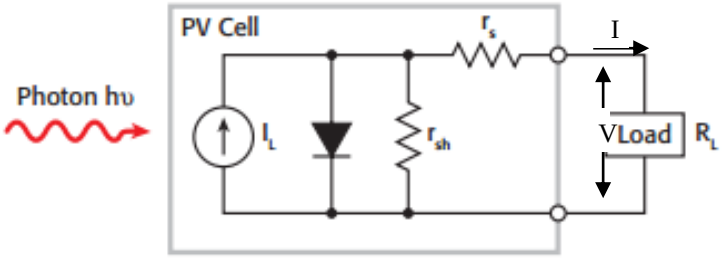

Figure 2 Equivalent circuit of a real PVC under the light.

The I_{sc} is the current passerby of the cell at zero utilized voltage; near-zero polarization, the slope is an R_{sh} value that matches the diode leaks [40].

Let us assume that: ($R_s = 0$; $R_{sh} = \infty$) with ($I = 0$; $I_L = I_{sc}$), the V_{oc} is determined by:

$$V_{oc} = \frac{nkT}{e} ln\left(\frac{I_{sc}}{I_s} + 1\right) \quad (10)$$

As well, the V_{oc} can be calculated by this analytical equation [34]:

$V_{oc} = E_{LUMO} - E_{CB}$

Then, I_{sc} decreased by the R_s, a small R_{sh} will decrease V_{oc} and the cell will not liberate any voltage within weak illumination *G*.

Operating principe of a DSS*C*

S: Sensitizer; S*: Electronically excited state; Iodide: a mediator.

The operating cycle can be summarizing in the terminology of the following chemical reactions [40]:

Anode: $S + h\upsilon \longrightarrow S^*$

Injection of electrons: $S^* \longrightarrow S^+ + e^- (TiO_2)$

Dye reduction: $2S^+ + 3I^- \longrightarrow 2S + I^{3-}$

Cathode regeneration: $I^{3-} + 2e^- (Pt) \longrightarrow 3I^-$

Calculation methods

In this work, our calculations were optimized in the gas phase by density functional theory (DFT) investigation with 6-31G(d,p) Gaussian basis sets [41,42] and B3LYP hybrid [43-45]. The oscillator force *f* and excited-state energy were determined using the TD-DFT/CAM-B3LYP processes in chloroform solvent. The integral equation formalism polarizable continuum model (IEF-PCM) was used in excitation energy [46-49]. The compounds' cationic and anionic states have been calculated at B3LYP/6-311G(d,p) level to determine the λ_{total}.

Experimental

Materials

All the reagents and solvents used for the preparation of these compounds were published in previous work [50]. NMR spectra were performed on a BRUKER AM 300 spectrometer operating in Fourier transform at a frequency of 300.13 MHz for 1 H NMR and 75.47 MHz for 13 C NMR. The associated calculator uses an Aspect 3000 using the BRUKER 1986 software (DI6R 861). The compounds were dissolved in a deuterated solvent (DMSO or CDCl3). Tetramethylsilane (TMS) is used as a fictitious reference.

Synthesis of organic compounds

These compounds were synthesized from quinoxaline derivatives (**A**-**D**), and 5-chlorométhyl-8-hydroxyquinoline hydrochloride (**5-CMHQ**) using a technically simple method, and with very good yields (**Scheme 1**). 5-Chlorométhyl-8-hydroxyquinoline hydrochloride (**5-CMHQ**) was synthesized from 8-hydroxyquinoline (**HQ**) according to a method described in previous work [51]. Their structures were characterized by ^{1}H and ^{13}C NMR spectroscopy.

The reaction for the synthesis of new quinoxaline based on 8-hydroxyquinoline realized according to the following procedure:

A mixture of (0.01 moles) of alkylquinoxaline (A-D) and (0.02 moles) of 5-chloromethyl-8-hydroxyquinoline hydrochloride (5-CMHQ) in 50 mL of tetrahydrofuran (THF) in the presence of (0.03 moles) of triethylamine (Et_3N) is brought to reflux under magnetic stirring for 24 h. The monitoring of the reaction was controlled by TLC using a dichloromethane/hexane mixture (85:15, v/v). When the reaction ends, the solvent was evaporated, and the residue obtained was dissolved in 20 mL of water, and extracted with dichloromethane (3×20 ml). The organic phases are combined, washed twice with a saturated aqueous solution of NaCl, dried over anhydrous $MgSO_4$, and evaporated on a rotary evaporator under the vacuum

of the water pump. The crude product obtained is washed with acetone, and purified by chromatography on a silica gel column using the dichloromethane/hexane mixture (85:15, v/v). The obtained chromatographed product was recrystallized from absolute ethanol.

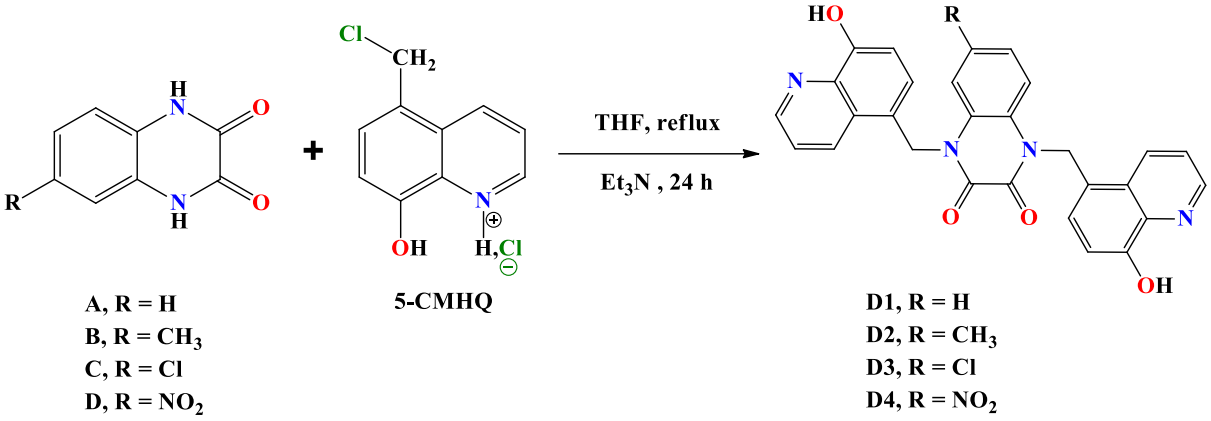

Scheme 1 Synthetic route for the synthesis of **D1-D4**.

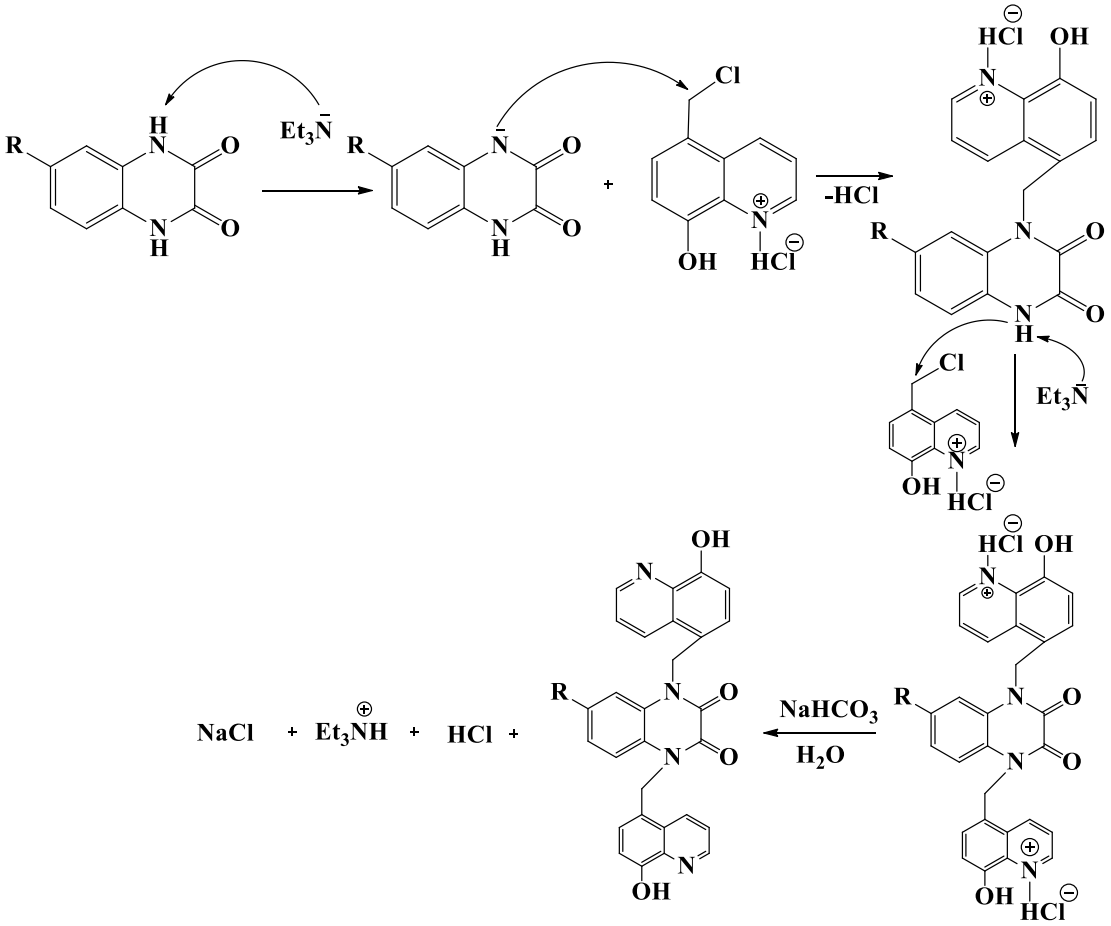

Scheme 2 Mechanism of the N-alkylation of 5-chloromethyl-8-hydroxyquinoline hydrochloride by 6-alkylquinoxalein-2,3-diones derivatives

Results and discussion

Experimental study

Organic synthesis (Data value and validation)

D1: ^{1}H NMR ($CDCl_3$) 4.85 (s, 2 H, OH), 5.37 (s, 2 H, CH_2), 7.48-8.77 (m, 2 H, ArH-quinoxaline), 7.10-7.45-7.45-8.48-8.77 (m, 10 H, ArH-quinoline). ^{13}C NMR (DMSO): 46.08 (CH_2), 150.67 (ArC-OH), 153.86 (C=O) 127.03-122.95 (ArCH-benzene of quinoxaline), 131.18 (ArC-benzene of quinoxaline), 112.87-121.24-127.80-131.18-148.27 (ArCH-quinoline), 122.66-128.24-127.18 (ArC-quinoline).

D2: ^{1}H NMR ($CDCl_3$) 2.37 (s, 3 H, CH_3), 5.33 (s, 2 H, OH), 3.91 (s, 2 H, CH_2), 7.04-7.04-7.06-7.41-7.46 (m, 10 H, ArH-quinoline), 6.54-7.09-7.25 (m, 3 H, ArH-quinoxaline). ^{13}C NMR (DMSO) 46.12 (CH_2), 21.57 (CH_3), 151.00 (ArC-OH), 152.86 (C=O) 121.77-111.23-130.30 (ArCH-benzene of quinoxaline), 128.35-133.93 (ArC-benzene of quinoxaline), 110.74-122.77-126.91-128.76-148.09 (ArCH-quinoline), 125.97-128.35-138.76 (ArC-quinoline).

D3: ^{1}H NMR (DMSO-d_6): 4.68 (s, 1 H, OH), 4.55 (s, 2 H, CH_2), 7.04-7.23-7.60-8.83-9.08 (m, 5 H, ArH-quinoline), 7.18-7.19-7.21-7.51 (m, 4 H, ArH-quinoxaline). ^{13}C NMR (DMSO-d_6): 52.39 (CH_2), 151.16 (ArC-OH), 151.36 (C=O), 114.08-123.38-129.23-130.12-144.99 (ArCH-quinoxaline), 130.26-144.54 (ArC-quinoxaline), 111.14-117.70-126.57-128.92-144.99 (ArCH-quinoline), 126.30-128.41-135.55 (ArC-quinoline).

D4: ^{1}H NMR (DMSO-d_6): 1.11 (s, 3 H, CH_3), 6.99 (s, 1 H, OH), 4.73 (s, 2 H, CH_2), 7.02-7.34-7.53-7.58-7.61 (m, 10 H, ArH-quinoline), 7.19-7.20-7.50-7.57 (m, 3 H, ArH-quinoxaline). ^{13}C NMR (DMSO-d_6) 23.64 (CH_3), 152.49 (ArC-OH), 168.62 (C=O), 127.47-132.09-133.51-148.12 (ArCH-benzene), 127.57-138.21-139.38 (ArC-benzene), 111.05-122.06-126.28-130.54-134.88 (ArCH-quinoline), 125.60-128.73-137.20 (ArC-quinoline).

The ^{1}H NMR spectra of the compounds **D1-D4** taken in the DMSO-d6, show in particular the signals relating to the protons of the alkyl groups, thus highlighting the disappearance of the signals attributable to the **NH** groups; which attests to their commitment to the reaction. The ^{13}C NMR spectra of the compounds **D1-D4** taken in DMSO-d6, show the appearance of the signals relating to the secondary carbons linked to the nitrogen atoms of the quinoxaline compounds.

The secondary nitrogen atoms of the quinoxaline compounds are polarized δ^- and their non-binding doublets have a nucleophilic character, which allows the attack on the carbon atom carrying the chlorine of the compound **5-CMHQ**.

Theoretical study

Geometry structures

The investigation for every molecule's chemical structure presented in **Figure 1** appear that they have a similar coplanar structure. The coplanar composed-conformation should improve the electron transfer from e^--D to e^--A through the π-spacer unit for our compounds.

CAM-B3LYP method was applied and reasonably able to predict the excitation energies and absorption spectra of D-A compounds [52,53]. So, vertical excitation energy and electron absorption spectrum stimulated by TD-CAM-B3LYP process.

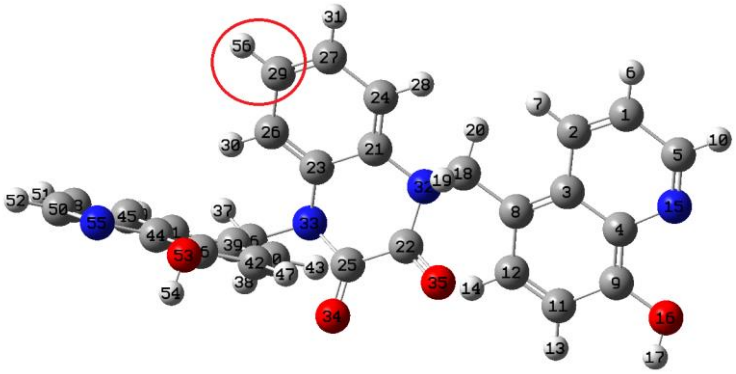

Figure 3 Optimized representations of the molecule D1 and the positions of each atom.

This study makes it possible to give results on optimized structural parameters: The interatomic distances, the valence angles and the dihedral angles, **Table 1** illustrates the results found for the 4 compounds Di (i = 1 - 4).

Table 1 Bond lengths, valence angles and dihedral angles of the used compounds.

Compound	D_1	D_2	D_3	D_4
C29-R56 (Å)	1.084	1.512	1.822	1.459
C27-C29-R56 (°)	119.51	120.66	118.59	118.56
C24-C27-C29-R56 (°)	−179.20	−179.69	179.74	179.65

From **Table 1**, the comparative study between the 4 molecules showed that the 2 structural parameters, valence angles and dihedral angles are very similar to the base molecule with a difference in binding length. Effectively, the π-conjugated group in this D-π-A shape, is employed as a surface from intramolecular charge transfer ICT of e^--D to e^--A group. The bond lengths for all molecules notably decreasing in similitude along those in S_0, which is important for absorption spectra, that A-group and π-bridge (quinoxalinedione) linking is very important for enhanced ICT characteristic.

Intramolecular charge transfer

Intramolecular charge transfer (ICT) was obtained by using frontier molecular orbital (FMO). The LUMO and HOMO electron locative distribution are presenting in **Figure 4** of all molecules. Therefore, the HOMO and LUMO plots confirmed the π-type characteristics MO typical. The HOMO presents an anti-bonding type between bonding type and 2 adjacent fragments for each unit; on the other hand, LUMO exhibits a bonding type between 2 adjacent fragments. Thus, the lowest-lying singlet states are corresponding to ππ* character electronic transition. The LUMOs and HOMOs pattern is like with every other (**Figure 4**). The HOMOs electron propagation is principally situated in e^--D to π-conjugated space, whereas the LUMOs are primarily positioned in e^--A fragments and conjugation spacing half. Therefore, all D-π-A compounds e^- transitions from HOMO to LUMO it can lead to ICT from Donor-units to Acceptor-anchoring groups through a conjugated bridge, so the HOMO–LUMO displacement possibly classified as a ππ* ICT. All compounds C=O-anchoring groups have remarkable participation to LUMOs who grant a solid electronic coupling with TiO_2 area, thereby improving the e^--injection performance and subsequently enhance the J_{sc}.

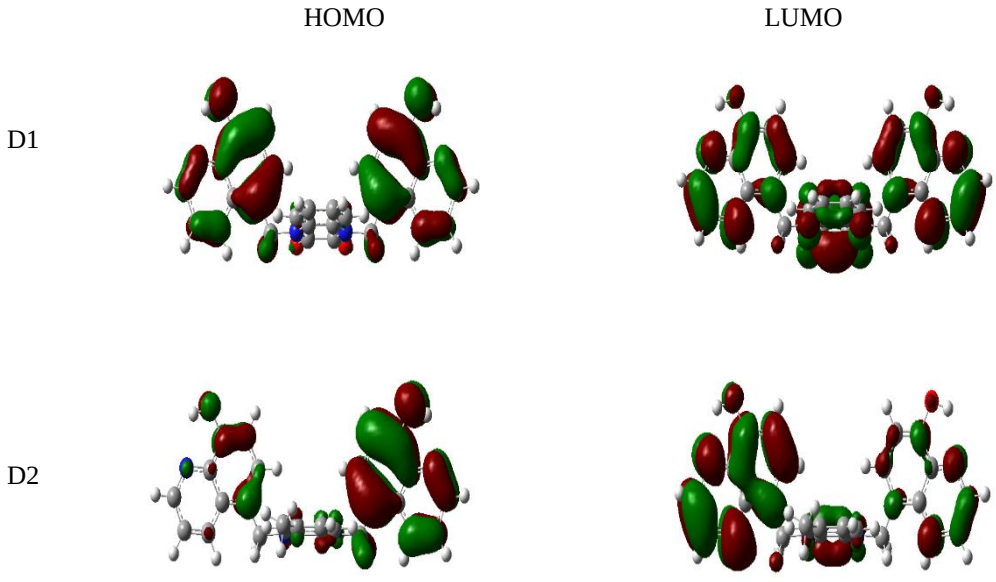

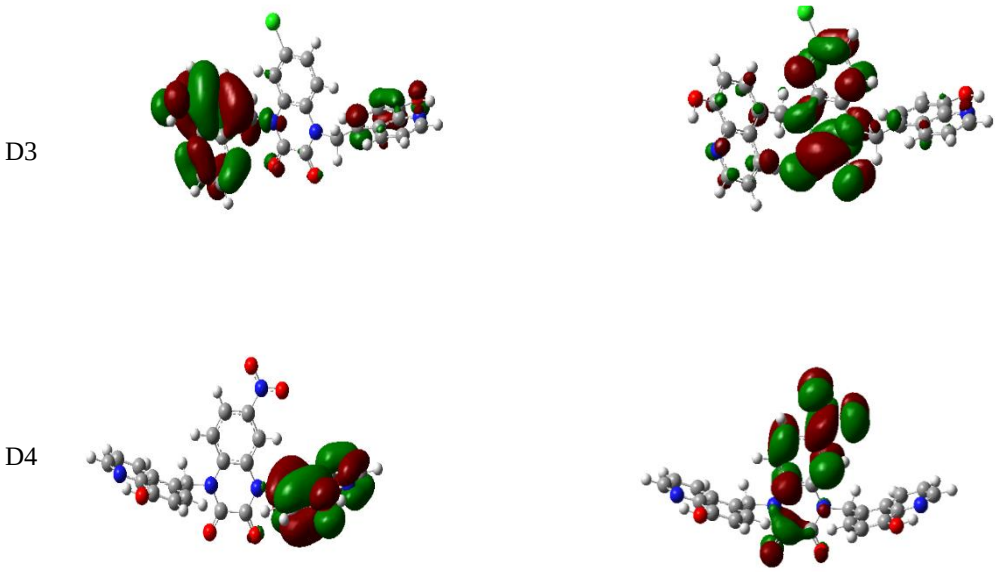

Figure 4 All compounds frontier orbital contour plots.

Molecular orbitals

A D-π-A compound with a stronger e⁻-D group as compared to that with a weaker e⁻-D group, usually give a high HOMO. The e⁻-D impact on the electronic properties is calculated using different D groups. HOMO energies of the 4 dyes are increasing in order of D1 → D2 → D3 → D4. Since D1 has the highest HOMO value (−5.947 eV), it contains the strongest e⁻-D group. D2, D3 and D4 with investigated E_{HOMO} respectively −7.235, −7.366 and −7.374 eV, have a weak input in e⁻-D ability because they restrict a group in e⁻-D moiety. In **Figure 5** the calculated LUMO energies from all sensitizers are relative without influence by variations in molecular structure, owing to a little e⁻-A group (C=O) impaction, which is less affected by D-group changing. The ΔE_g results are presenting in **Figure 5**, thus ΔE_g are increasing in order of D1 → D4 → D3 → D2. The ΔE_g ranges are about 4.110-6.626 eV; consequently, these molecules can be used in DSSC applications.

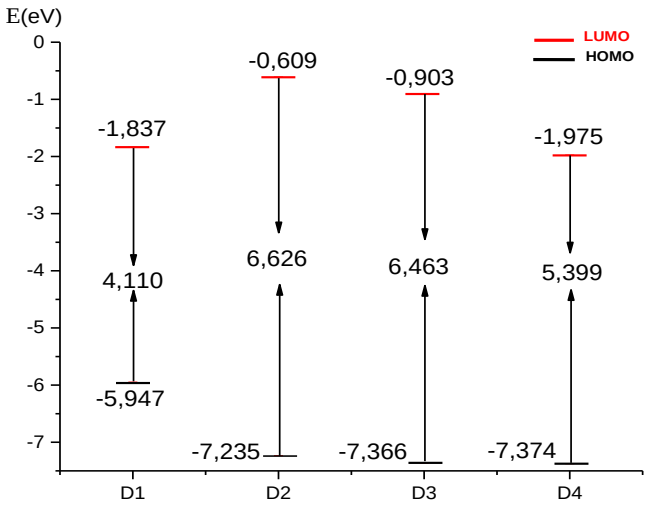

Figure 5 Schematic energy diagram of all molecules utilized.

Optical properties

Optical properties were obtained in the chloroform solution of all sensitizers [54,55]. The chloroform was employed in UV-Visible absorption between 280 and 360 nm as a solvent on quinoxalinedione-based molecules; a similar outline for all dyes is indicated in the spectrum (**Figure 6**). The gap HOMO-LUMO position and the first band largeness in the spectrum are the 2 first parameters that can be related to the dye efficiency, for reduce energies favors the light-harvesting process. The first vertical excitation energies (E_{ve}) of our dyes are decreasing in order of D1 → D4 → D2 → D3. Compared with D3, the D4 and D2 absorption spectrum show slightly blue shift with decreasing oscillator strength, due probably to the heteroatom electronegativity existence in the e^--D groups. D1, D4, D2 and D3 absorption spectra present the main peak at ~297, 265, 252 and 240 nm, respectively.

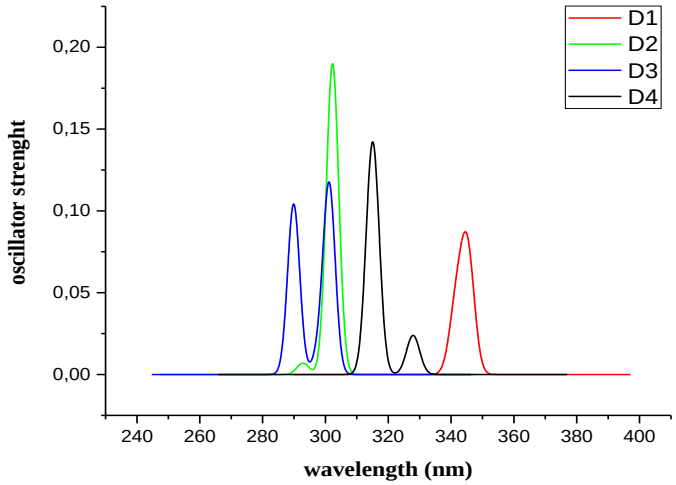

Figure 6 Absorption spectra of all dyes Di (i = 1 - 4).

In adiabatic measure, the emission spectra were determined to discuss the molecules photoluminescence characters of all dyes. **Table 2** present the dyes optical properties including the calculated fluorescence wavelengths with the strongest oscillator. For these dyes, the emission spectra appearing from S_1 state is assigned to LUMO→HOMO character and π*→π transition, we found that the calculated fluorescence is only the lowest-lying absorption reverse process. Moreover, the red shift fluorescence spotted of photoluminescence spectra is increasing in order of D1 → D4 → D2 → D3; well good according to the absorption observed data when passing from D3 to D1. The D3, D2 and D1 emitted at higher wavelengths (301.19, 302.79 and 345.44 nm) with strongest intensity (f = 0.115, f = 0.074 and f = 0.037). These encouraging optical properties suggest that D3 with chlorine group could be the best recommended in the DSSC.

Table 2 Optical properties of all days Di(i = 1 - 4) obtained by CAM-B3LYP/6-311G (d.p).

Day	E_{00} (eV)	E_{HOMO} (eV)	E_{LUMO} (eV)	ΔE (eV)	λ_{max} (nm)	f	E_T (eV)	μ (Debye)
D1	3.5892	−5.947	−1.837	4,11	345.44	0.037	−1598.39	8.318
D2	4.0947	−7.235	−0.609	6,626	302.79	0.074	−1636.84	9.030
D3	4.1165	−7.366	−0.903	6,463	301.19	0.115	−2057.28	4.520
D4	3.4442	−7.374	−1.975	5,399	359.98	0.000	−1801.93	6.397

In this part, the dipole moment vectors in a 3D representation of all dyes Di (i = 1 - 4) were determined by the theoretical calculation method B3LYP 6-311G (d, p). **Figure 7** represents each dye with its dipole moment vector, the dipole moment vector μ was compared to the standard orientation for each compound, i.e. that the center in each nuclear charge is the coordinates origin [4,5]. The dipole moment vectors in a 3D figuration of our 4 quinoxalinedione derivatives were presented in **Figure 7**; the μ for D1 (8.318 D) increased slightly in D2 and decreased slightly in D4, with a weak orientation, and decreased in D3 (4.520 D) with an important orientation. Moreover, the dipole moment variations in D2 case are greatly smaller in comparison with that appear in D3 and D4, the electronegative (chlorine and nitro) existence in the same position, not only decreased dramatically the dipole moment but as well modified the vector orientation with large angle (~34° in D4 and ~85° in D3). The NPA charges present an indication as well as this change to μ are in according with known low eligibility impact of nitro and chlorine, previously recognized [43,47,56,57], as compared to its inductive impact.

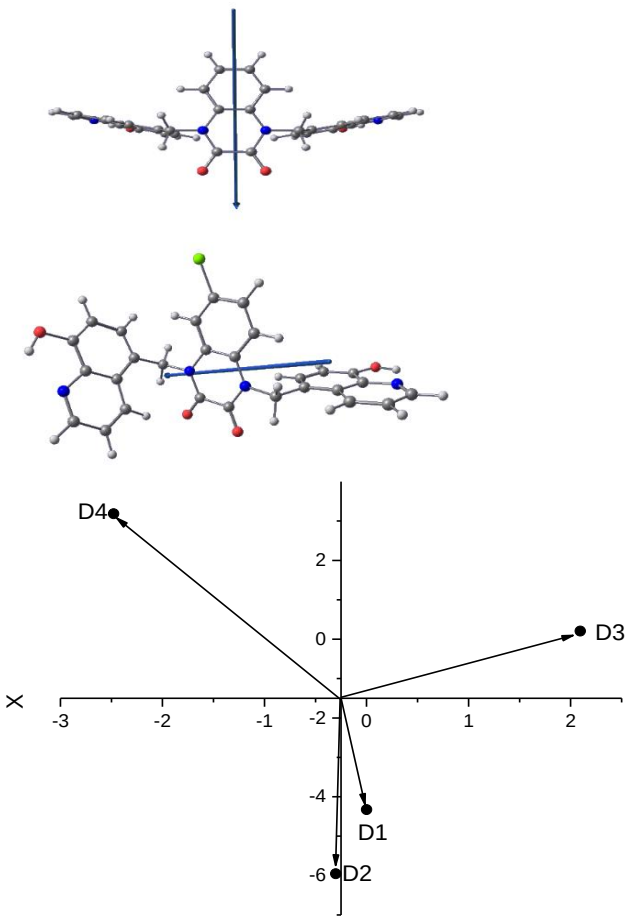

	X	Y	Z
D1	0.0003	−4.3263	7.1048
D2	−0.3008	−5.9541	6.7829
D3	2.0946	0.2069	4.0001
D4	−2.4787	3.1858	4.9631

Figure 7 Dipole moments vectors in a 3D figuration for all days, calculated by B3LYP 6-311G.

Photovoltaic properties

The E^{dye} value was determined as negative E_{HOMO} [39]; E^{dye*} is estimated, E^{dye*} of all molecules are increased in order of D2 → D3 → D4 → D1. Thus, the most practical oxidizing species are D2 and D3 while D1 is the worst. For every dye, all ΔG^{inject} obtained are negative, as well the e^- injection from compound to TiO_2 are impulsive.

As seen in **Figure 8** and **Table 3**, the $-\Delta G^{inject}$ are decreased in order of D2 → D3 → D4 → D1. This presents that D2 and D3 have the greatest $-\Delta G^{inject}$ value, while D1 has the littlest. The LHE result has to be as high as possible to expand the photocurrent answer. For these molecules, LHE is in a close range 0.0-0.232 with slight growth, so that all these sensitizers present similar photocurrent.

Table 3 Electrochemical parameters for all used compounds.

Dye	E^{dye} (eV)	E^{dye*} (eV)	ΔG^{inject} (eV)	LHE	λ_h (eV)	λ_e (eV)	λ_{total} (eV)	V_{oc} (eV)
D1	1.837	−4.110	−7.6992	0.0816	0.18020	0.35565	0.53584	2.163
D2	0.609	−6.626	−10.7207	0.1560	0.18340	0.18478	0.36818	3.391
D3	0.903	−6.463	−10.5795	0.2320	0.15987	0.25395	0.41382	3.097
D4	1.975	−5.399	−8.8432	0	0.18819	0.29105	0.47924	2.025

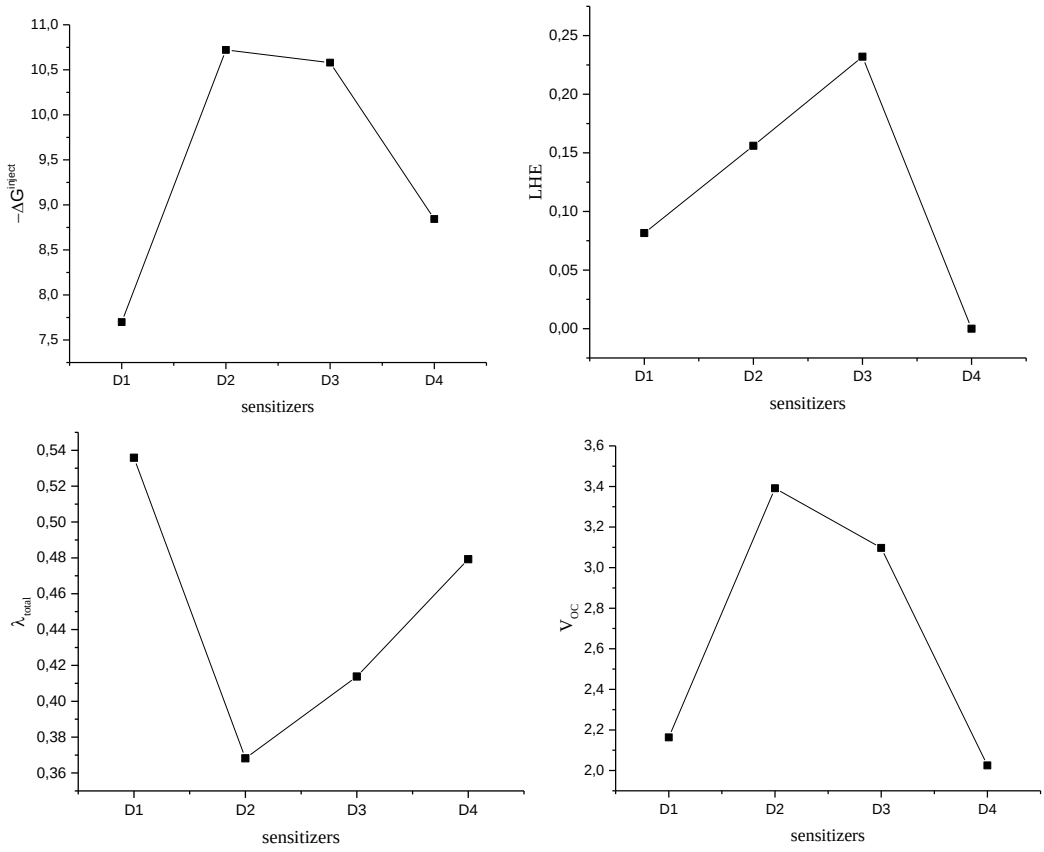

Figure 8 Critical parameters influenced J_{sc} along of calculated sensitizers: ΔG^{inject}, LHE, λ_{total} and V_{oc}.

Consequently, compounds D2 and D3 show a favorable J_{sc}, important LHE, larger ΔG^{inject} and smaller λ_{total}; and mostly ΔG^{inject} and λ_{total} are more important to govern the J_{sc}.

In addition, the overall power conversion efficiency η could be affected as well by V_{oc}. Therefore, for these 2 molecules, the electron injection is more efficient for these sensitizers with the larger excited state related to the band edge of semiconductor conduction, ie. higher V_{oc}. It was found that V_{oc} of all compounds is in the range 2.025 - 3.391 eV and decreasing in order of D2 → D3 → D1 → D4. It shows that D3 and D2 have the higher V_{oc} than other compounds, while D4 has the smallest.

In addition, the LHE as well could allocate the electron injection kinetics. Consequently, the calculated LHE is as well significant to analyze the relationship between electron structure and critical influenced parameter J_{sc}. Thus, in **Figure 7** and **Table 2** the calculated LHE of all compounds is increasing in order of D4 → D1 → D2 → D3. This shows that D4 have the smallest LHE but D3 have the largest.

Thus, we could draw a conclusion that the high LHE, $-\Delta G^{inject}$ and V_{oc} can give an important efficiency. Accordingly, the DSSC compound effectiveness by D3 dye might be favorable to the other sensitizers, because of its preferable effectiveness of the over parameters founded on our calculated results.

Conclusions

In this work, the synthesis and the characterization of a new series of heterocyclic compounds obtained by association of 8-hydroxyquinoline with quinoxalinedione derivatives were presented. The synthesis of this series of compounds was carried out by simple conditions but with good yields and the characterization data shows that there is good consistency between the spectroscopic data and the proposed structures. These new compounds were obtained according to simple procedures with good yields and they have been the subject of a theoretical study.

The intended results were investigating by DFT calculation with the CAM-B3LYP method. Since D2 and D3 dyes have the largest values of (LHE, $-\Delta G^{inject}$, V_{oc}) and have the smallest values of (λ_{total}). In comparison with other dyes, D2 and D3 compounds were founding to be the best photo-sensitizer for use in DSSC. Since these results are sufficient for an efficient e^- injection, D2 and D3 compounds can be used as organic solar cells except D1 and D4. Finally, this investigated process can be employed to predict the optical and photovoltaics properties on the other compounds and polymers, and it encourages synthesis of the novel organic solar cell materials.

Acknowledgments

This work was supported by “Hassan II University”, “Ibn Tofail University” and the “Moroccan CNRST,” Morocco. We are pleased to acknowledge them.

References

[1] M Alswah, AH Bayoumi, K Elgamal, A Elmorsy, S Ihmaid and HEA Ahmed. Design, synthesis and cytotoxic evaluation of novel chalcone derivatives bearing triazolo[4,3-a]-quinoxaline moieties as potent anticancer agents with dual EGFR kinase and tubulin polymerization inhibitory effects. *Molecules* 2018; **23**, 48.

[2] M Joshi, SK Pal and JJ Drabick. Novel approaches in cancer immunotherapy: A light at the end of the tunnel. *Dis. Med*. 2016; **21**, 479-87.

[3] B Mathew, JV Hobrath, MC Connelly, RK Guy and RC Reynolds. Diverse amide analogs of sulindac for cancer treatment and prevention. *Bioorg. Med. Chem. Lett*. 2017; **27**, 4614-21.

[4] I Ali, J Lee, A Go, G Choi and K Lee. Discovery of novel [1, 2, 4] triazolo [4, 3-a] quinoxaline aminophenyl derivatives as BET inhibitors for cancer treatment. *Bioorg. Med. Chem. Lett*. 2017; **27**, 4606-13.

[5] AE Assyry, B Benali, B Lakhrissi, ME Faydy, ME Touhami, R Touir and M Touil. Experimental and theoretical comparatives investigation of mild steel corrosion inhibition by quinoxalinone derivatives in 1 M HCl. *Res. Chem. Intermed.* 2015; **41**, 3419-31.

[6] F Benhiba, Y ELaoufir, M Belayachi, H Zarrok, AE Assyry, A Zarrouk, B Hammouti, EE Ebenso, A Guenbour, SSA Deyab and H Oudda. Theoretical and experimental studies on the inhibition of 1,1â-(2-phenylquinoxaline-1,4-diyl) diethanone for the corrosion of carbonsteel in 1.0 M HCl. *Der Pharm. Lett.* 2014; **6**, 306-18.

[7] M Larouj, Y ELaoufir, H Serrar, AE Assyry, M Galai, A Zarrouk, B Hammouti, A Guenbour, AE Midaoui, S Boukhriss, ME Touhami and H Oudda. Inhibition effects and theoretical studies of novel synthesized pyrimidothiazine derivative as corrosion inhibitor for carbon steel in phosphoric acid solution. *Der Pharm. Lett.* 2014; **6**, 324-34.

[8] A Chaouiki, M Chafiq, M Rbaa, H Lgaz, R Salghi, B Lakhrissi, IH Ali, S Masroor and Y Cho. New 8-hydroxyquinoline-bearing quinoxaline derivatives as effective corrosion inhibitors for mild steel in HCl: electrochemical and computational investigations. *Coatings* 2020; **10**, 811.

[9] M Rbaa, M Galai, ME Faydy, Y Lakhrissi, ME Touhami, A Zarrouk and B Lakhrissi. Synthesis and characterization of new quinoxaline derivatives of 8- hydroxyquinoline as corrosion inhibitors for mild steel in 1.0 M HCl medium. *J. Mater. Environ. Sci*. 2018; **9**, 172-88.

[10] AE Assyry, B Benali, R Jdaa, B Lakhrissi, M Touil and A Zarrouk. Theoretical investigation using AMYR calculations of five quinoxalinones in interaction with water molecules. *J. Mater. Environ. Sci.* 2014; **5**, 1434-41.

[11] Q Liu, Y Jiang, K Jin, J Qin, J Xu, W Li, J Xiong, J Liu, Z Xiao, K Sun, S Yang, X Zhang and L Ding. 18% Efficiency organic solar cells. *Sci. Bull.* 2020; **65**, 272-5.

[12] JH Schön, C Kloc and B Batlogg. Efficient photovoltaic energy conversion in pentacene-based heterojunctions. *Appl. Phys. Lett*. 2000; **77**, 2473-5.

[13] PL Barny, V Dentan, H Facoetti, M Vergnolle, G Vériot, B Servet and CR Acad. Application of organic electroluminescent materials in visualization. *Sci. Paris Sér.* 2000; **1**, 493.
[14] N Mariotti, M Bonomo, L Fagiolari, N Barbero, C Gerbaldi, F Bella and C Barolo. Recent advances in eco-friendly and cost-effective materials towards sustainable dye-sensitized solar cells. *Roy. Soc. Chem.* 2020; **22**, 7168-218.
[15] AAF Husain, WZW Hasan, S Shafie and SS Pandey. A review of transparent solar photovoltaic technologies. *Renew. Sustain. Energ. Rev*. 2018; **94**, 779-91.
[16] FC Krebs, SA Gevorgyan and J Alstrup. A roll-to-roll process to flexible polymer solar cells: model studies, manufacture and operational stability studies. *J. Mater. Chem*. 2009; **19**, 5442-51.
[17] FC Krebs, J Fyenbo and M Jørgensen. Product integration of compact roll-to-roll processed polymer solar cell modules: methods and manufacture using flexographic printing, slot-die coating and rotary screen printing. *J. Mater. Chem*. 2010; **20**, 8994-9001.
[18] K Sharma, V Sharma and SS Sharma. Dye-sensitized solar cells: Fundamentals and current status. *Nanoscale Res. Lett.* 2018; **13**, 381.
[19] Q Fan, Q An, Y Lin, Y Xia, Q Li, M Zhang, W Su, W Peng, C Zhang, F Liu, L Hou, W Zhu, D Yu, M Xiao, E Moons, F Zhang, TD Anthopoulos, O Inganas and E Wang. Over 14% efficiency all-polymer solar cells enabled by a low bandgap polymer acceptor with low energy loss and efficient charge separation. *Energ. Environ. Sci*. 2020; **13**, 5017-27.
[20] YY Liang, Z Xu, JB Xia, ST Tsai, Y Wu, G Li, C Ray and LP Yu. For the bright future-bulk heterojunction polymer solar cells with power conversion efficiency of 7.4%. *Adv. Mater.* 2010; **22**, E135-E138.
[21] KL Mutolo, EI Mayo, BP Rand, SR Forrest and ME Thompson. Enhanced open-circuit voltage in subphthalocyanine/C60 organic photovoltaic cells. *J. Am. Chem. Soc.* 2006; **128**, 8108-9.
[22] A Gadisa, M Svensson, MR Andersson and O Ingana. Correlation between oxidation potential and open-circuit voltage of composite solar cells based on blends of polythiophenes/ fullerene derivative. *Appl. Phys. Lett*. 2004; **84**, 1609-11.
[23] SH Chan, CP Chen, TC Chao, C Ting, CS Lin and BT Ko. Synthesis, characterization, and photovoltaic properties of novel semiconducting polymers with thiophene-phenylene-thiophene (TPT) as coplanar units. *Macromolecules* 2008; **41**, 5519-26.
[24] AE Assyry, A Hallaoui, F Abrighach, R Touzani, A Zarrouk and A Lamhamd. DFT spectroscopy properties of new N-heterocyclic compounds designed for efficient photovoltaic applications. *Der Pharm. Lett.* 2015; **7**, 151.
[25] HX Ji, ZS Huang, L Wang, D Cao. Quinoxaline-based organic dyes for efficient dye-sensitized solar cells: Effect of different electron-withdrawing auxiliary acceptors on the solar cell performance. *Dyes Pigm.* 2018; **159**, 8-17.
[26] AE Assyry, R Jdaa, B Benali, M Addou and A Zarrouk. Optical and photovoltaic properties of new quinoxalin-2 (1H)-one-based DA organic dyes for efficient dye-sensitized solar cell using DFT. *J. Mater. Environ. Sci*. 2015; **6**, 2612-23.
[27] A Dessì, GB Consiglio, M Calamante, G Reginato, A Mordini, M Peruzzini, M Taddei, A Sinicropi, ML Parisi, FF Biani, R Basosi, R Mori, M Spatola, M Bruzzi, L Zani. Organic chromophores based on a fused bis-thiazole core and their application in dye-sensitized solar cells. *Eur. J. Org. Chem*. 2013; **2013**, 1916-28.
[28] L Sicot, C Fiorini, A Lorin, P Raimond, C Sentein, JM Nunzi. Improvement of the photovoltaic properties of polythiophene-based cells. *Sol. Energ. Mater Sol. Cells.* 2000; **63**, 49-60.
[29] JM Nunzi. Organic photovoltaic materials and devices. *Compt. Rendus. Phys.* 2002; **3**, 523-42.
[30] J Rostalski and D Meissner. Monochromatic versus solar efficiencies of organic solar cells. *Solar Energ. Mater. Solar Cells* 2000; **61**, 87-95.
[31] YS Ang, Y Chen, C Tan and LK Ang. Generalized high-energy thermionic electron injection at graphene interface. *Phys. Rev. Appl.* 2019; **12**, 014057.
[32] ZL Zhang, LY Zou, AM Ren, YF Liu, JK Feng and CC Sun. Theoretical studies on the electronic structures and optical properties of star-shaped triazatruxene/heterofluorene co-polymers. *Dyes Pigm*. 2013; **96**, 349-63.
[33] JB Asbury, YQ Wang, E Hao, H Ghosh and T Lian. Evidences of hot excited state electron injection from sensitizer molecules to TiO2 nanocrystalline thin films. *Res. Chem. Intermed*. 2001; **27**, 393-406.
[34] J Zhang, HB Li, SL Sun, Y Geng, Y Wu and ZM Su. Density functional theory characterization and design of high-performance diarylamine-fluorene dyes with different π spacers for dye-sensitized solar cells. *J. Mater. Chem*. 2012; **22**, 568-76.

[35] AE Assyry, A Hallaoui, A Zarrouk, ME Hezzat, M Assouag, S Boukhris and MME Touhami. Photophysical study by density functional theory for photovoltaic effects of some quinoxaline derivatives. *Der Pharm. Chem*. 2015; **7**, 128-38.
[36] WL Ding, DM Wang, ZY Geng, XL Zhao and WB Xu. Density functional theory characterization and verification of high-performance indoline dyes with D–A–π–A architecture for dye-sensitized solar cells. *Dyes Pigm.* 2013; **98**, 125-35.
[37] W Sang-aroon, S Saekow and V Amornkitbamrung. Density functional theory study on the electronic structure of Monascus dyes as photosensitizer for dye-sensitized solar cells. *J. Photochem. Photobiol. A* 2012; **236**, 35-40.
[38] MP Balanay and DH Kim. DFT/TD-DFT molecular design of porphyrin analogues for use in dye-sensitized solar cells. *J. Mol. Struct.* 2009; **910**, 20-6.
[39] AE Assyry, M Lamsayah, I Warad, R Touzani, F Bentiss and A Zarrouk. Theoretical investigation using DFT of quinoxaline derivatives for electronic and photovoltaic effects. *Heliyon* 2020; **6**, e03620.
[40] S Zhang. 2017, Study of fluorine-doped tin oxide (FTO) thin films for photovoltaics applications. Ph. D. Dissertation, Université Grenoble Alpes, Grenoble, France.
[41] JG Hill. Gaussian basis sets for molecular applications. *Int. J. Quantum Chem*. 2013; **113**, 21-34.
[42] RJ Magyar and S Tretiak. Dependence of spurious charge-transfer excited states on orbital exchange in TDDFT: large molecules and clusters. *J. Chem. Theory. Comput*. 2007; **3**, 976-87.
[43] MJ Frisch, GW Trucks, HB Schlegel, MJ Frisch, GW Trucks, HB Schlegel, GE Scuseria, MA Robb, JR Cheeseman, G Scalmani, V Barone, B Mennucci and GA Petersson. *Gaussian 09, revision A.02*. Gaussian, Pennsylvania, 2009.
[44] AE Assyry, A Hallaoui, R Saddik, N Benchat, B Benali and A Zarrouk. Combined electrochemical and quantum chemical study of new quinoxaline derivative as corrosion inhibitor for carbon steel in acidic media. *Der Pharm. Lett.* 2015; **7**, 295-304.
[45] AE Assyry, B Benali, A Boucetta and B Lakhrissi. Quantum chemical study by Density Functional Theory (DFT) of some benzodiazepine derivatives. *J. Mater. Environ. Sci.* 2014 ; **5**, 1860-7.
[46] J Tomasi, B Mennucci and R Cammi. Quantum mechanical continuum solvation models. *Chem. Rev*. 2005; **105**, 2999-3094.
[47] AE Assyry, B Benali, A Boucetta and D Mondieig. Synthesis and structural study of N-isopropenylbenzimidazolone. *Res. Chem. Intermed.* 2014; **40**, 1043-52.
[48] M Cossi and V Barone. Ab initio study of solvated molecules: A new implementation of the polarizable continuum model. *J. Chem. Phys*. 2001; **115**, 4708-17.
[49] C Adamo and V Barone. Toward reliable adiabatic connection models free from adjustable parameters. *Chem. Phys. Lett*. 2000; **330**, 152-60.
[50] M Rbaa, A Hichar, O Bazdi, Y Lakhrissi, K Ounine and B Lakhrissi. Synthesis, characterization, and in vitro antimicrobial investigation of novel pyran derivatives based on 8-hydroxyquinoline. *J. Basic Appl. Sci.* 2019; **8**, 8
[51] M Rbaa, H Lgaz, YE Kacimi, B Lakhrissi, F Bentiss and A Zarrouk. Synthesis, characterization and corrosion inhibition studies of novel 8-hydroxyquinoline derivatives on the acidic corrosion of mild steel: Experimental and computational studies. *Mater. Discov*. 2018; **12**, 43-54.
[52] D Mondieig, P Negrier, JM Leger, L Lakhrissi, AE Assyry, B Lakhrissi, EM Essassi, B Benali and A Boucetta. Synthesis and structural study of N-isopropenylbenzimidazolone. *Russ. J. Phys. Chem. A* 2015; **89**, 807-11.
[53] P Négrier, D Mondieig, JM Léger, B Benali, Z Lazar, A Boucetta, A Elassyry, B Lakhrissi, C Jermoumi and M Massoui. Crystal structure of benzodiazepin-2, 4-dione. *Anal. Sci.* 2006; **22**,175-6.
[54] D Jacquemin, EA Perpete, I Ciofini and C Adamo. TD-DFT performance for the visible absorption spectra of organic dyes: conventional versus long-range hybrids. *Acc. Chem. Res*. 2009; **42**, 326-34.
[55] C Adamo and D Jacquemin. The calculations of excited-state properties with Time-Dependent Density Functional Theory. *Chem. Soc. Rev*. 2013; **42**, 845-56.
[56] AE Assyry and B Benali. Theoretical study of the interaction between benzodiazepine derivatives and water by use of AMYR calculations. *Res. Chem. Intermed.* 2014; **40**, 627-36.
[57] KOK Al-Masoodi, I Rafiq, AE Assyry and A Derouiche. DFT/TD-DFT study of donorπ-acceptor organic dye models contained triarylamine for an efficient dye-sensitized solar cell. *J. Phys. Conf. Ser*. 2021; **1963**, 012012.